Isometric Spiracular Scaling in Scarab Beetles: Implications for Diffusive and Advective Oxygen Transport

Julian M. Wagner[1], C. Jaco Klok[1], Meghan E. Duell[1], John J. Socha[2], Guohua Cao[3], Hao Gong[4], Jon F. Harrison[1]

[1]*School of Life Sciences, Arizona State University, Tempe, AZ 85287-4501, USA*

[2]*Department of Biomedical Engineering and Mechanics, Virginia Tech, VA 24061, USA*

[3]*School of Biomedical Engineering, ShanghaiTech University, Shanghai 201210, CHINA*

[4]*Department of Radiology, Mayo Clinic, MN 55902, USA*

Short title: Spiracle scaling of beetles

Corresponding author: Jon Harrison, School of Life Sciences, Arizona State University, Tempe, AZ 85287-4501 USA, +1 (480)-965-9459; j.harrison@asu.edu

Abstract

The scaling of respiratory structures has been hypothesized to be a major driving factor in the evolution of many aspects of animal physiology. Here we provide the first assessment of the scaling of the spiracles in insects using ten scarab beetle species differing 180x in mass, including some of the most massive extant insect species. Using X-ray microtomography, we measured the cross-sectional area and depth of all eight spiracles, enabling the calculation of their diffusive and advective capacities. Each of these metrics scaled with geometric isometry. Because diffusive capacities scale with lower slopes than metabolic rates, the largest beetles measured require 10-fold higher PO_2 gradients across the spiracles to sustain metabolism by diffusion compared to the smallest species. Large beetles can exchange sufficient oxygen for resting metabolism by diffusion across the spiracles, but not during flight. In contrast, spiracular advective capacities scale similarly or more steeply than metabolic rates, so spiracular advective capacities should match or exceed respiratory demands in the largest beetles. These data illustrate a general principle of gas exchange: scaling of respiratory transport structures with geometric isometry diminishes the potential for diffusive gas exchange but enhances advective capacities; combining such structural scaling with muscle-driven ventilation allows larger animals to achieve high metabolic rates when active.

Keywords

Spiracle, scaling, Scarabaeidae, tracheal system, body size, oxygen transport

MAIN TEXT

Introduction

As animal species evolve different sizes, many aspects of their physiology and morphology scale disproportionately with one another (allometrically) with consequences for animal behavior, life history, evolution, and diversity (1-3). A driver of this disproportionality lies in the nonlinear scaling of geometry: doubling the radius of a sphere gives quadruple the surface area and octuple the volume; in a similar way, scaling up a small body plan gives drastically altered ratios of surface area, volume, and body length. Since the challenges associated with changes in body size have a geometric origin, they are ubiquitous. As a result, understanding the mechanisms animals use to overcome the effects of changes in geometric proportions remains a pervasive, important, and challenging biological problem. Three related aspects of animal function modulated by allometry are scaling of animal metabolic rates, often scaling with mass$^{0.75}$ (4, 5), limits on the maximal body sizes of specific taxa (6, 7), and gas exchange strategies (8). For gas exchange, volume of tissue and hence potential gas exchange needs of animals scale with the cube of length (like the sphere), while surface areas tend to scale with the square of length. This leads to a decline in the ratio of surface area to volume with size. As a consequence, when animals evolve larger sizes, they may need to adapt the proportions of their respiratory structures or increase the use of advection (bulk flow) to avoid facing limitations based on processes that depend more on surface area such as diffusion.

Limitations on the capacity of larger animals to support oxygen delivery to tissues have been proposed to drive the hypometric scaling of metabolic rates with size, as well as the hypometric scaling of many physiological (e.g., heart and ventilation rates) and

42 behavioral/ecological traits (e.g., territory size, dispersal distance) (1-4, 9). However, competing
43 theories suggest that other factors, such as heat dissipation constraints, nutrient uptake
44 constraints, or performance-safety trade-offs, drive the hypometric scaling of metabolic rates and
45 correlated variables, and that evolutionary adaptations of respiratory systems to size allow
46 animals to match oxygen supply to need regardless of body size (10-13). One important step in
47 resolving this controversy is determining how respiratory structures and mechanisms scale. The
48 vast majority of prior studies of the scaling of gas exchange structures have focused on
49 vertebrates, especially mammals. In contrast, there is relatively limited information on the
50 scaling of gas exchange structures in invertebrates, despite the fact that most animal species are
51 invertebrates (5, 14). The scaling of the insect respiratory system is of particular interest, as
52 aspects of tracheal system structure have been reported to scale hypermetrically, in contrast to
53 the isometric or hypometric scaling of respiratory structures in vertebrates, supporting the
54 hypothesis that possession of a tracheal respiratory system limits insect body size (6, 15-18).
55 Here, we report the first study of the scaling of insect spiracles, the gateway of air into the body
56 and the first step in oxygen delivery from air to tissues, presenting new insight into a key
57 morphological pathway in this most biodiverse clade of terrestrial animals.

58 Gas exchange usually occurs in a series of steps, often a sequence of alternating diffusive
59 and advective processes. The capacity for a respiratory surface to conduct oxygen (diffusive
60 conductance, G_{diff}) can be described using Fick's law, that is

61 $$(1)\ G_{diff} = \frac{\text{area}}{\text{thickness}} * K.$$

62 where K is Krogh's diffusion constant for oxygen in the barrier. The diffusive oxygen exchange
63 across the surface (J_{diff}, mol sec^{-1}) is given by

64 (2) $J_{diff} = G_{diff} * \Delta P_{O2}$.

65 where ΔP_{O2} is the partial pressure gradient for oxygen across the exchanger. When gas exchange
66 relies on diffusion across a barrier, either G_{diff} or ΔP_{O2} must increase to match the increased
67 oxygen demand inherent in a larger body size (a larger relative tissue volume), or oxygen supply
68 will limit metabolic rate. Increases in G_{diff} may be accomplished by either a decrease in diffuser
69 thickness or increase in area. The ΔP_{O2} from air to mitochondria can be no greater than
70 atmospheric P_{O2} (approximately 21 kPa at sea level); this biophysical constraint sets an upper
71 limit on the ability of large animals to utilize increases in ΔP_{O2} to overcome a G_{diff} that does not
72 increase in proportion to oxygen consumption rate.

73 The scaling of surface area, barrier thickness, and ΔP_{O2} for gas exchangers across species
74 of animals varies with clade and developmental stage. In adult vertebrates, the scaling of the
75 passive diffusing capacity of the lung across species scales hypometrically, but matches the
76 scaling of metabolic rates (5). However, the scaling of respiratory morphology differs in
77 endotherms and ectotherms (5), as barrier thickness is constant with size in ectotherms, but
78 increases with size in endotherms. As a consequence, endotherms must scale surface area of the
79 lung more steeply than ectotherms to account for their increased barrier thickness and match the
80 scaling of G_{diff} to the scaling of metabolic rate. Bird eggs, which rely on diffusion through pores
81 for oxygen, employ a different strategy. Eggs of larger species have relatively thicker shells
82 (scaling with $mass^{0.45}$), increasing barrier thickness with size, likely to mitigate a higher
83 likelihood of mechanical damage (19). Pore area increases proportionally with shell thickness, so
84 G_{diff} per pore is relatively constant across egg size, and larger eggs have a higher density of pores
85 (20). The scaling of the G_{diff} of the shell overall matches the scaling of metabolic rate across

86 species, with both scaling hypometrically (19, 20). Pycnogonids (sea spiders) show yet another
87 pattern for the diffusing capacity of their respiratory structures (their legs). Unlike either bird
88 eggs or vertebrate lung membranes, pycnogonid barrier thickness scales isometrically (7). As in
89 bird eggs, there is an increase in the area-specific diffusing capacity of the leg cuticle of larger
90 pycnogonids, although the morphological basis remains unclear (7). However, the increases in
91 diffusive conductance of the respiratory exchanger are not sufficient to match increases in
92 metabolic rates with size, so the ΔP_{O2} across the leg cuticle increases in larger pycnogonid
93 species, which may limit maximal species size in this taxa (7).

94 Advective steps in gas exchange can occur using either air or aqueous media and
95 represent a second broad strategy for delivering gases to tissues. The morphological capacity for
96 a structure to transport a fluid by advection, G_{adv}, m^4 s kg^{-1}, can be described from Poiseulle's
97 law,

98 (3) $$G_{adv} = \frac{\text{area}^2}{8 * \text{dynamic viscosity} * \text{length}}.$$

99 Given this relationship, the advective transport of oxygen through the structure (J_{adv}, mol sec^{-1}) is
100 is given by

101 (4) $J_{adv} = G_{adv} * [O_2] * \Delta HP.$

102 where $[O_2]$ is the concentration of O_2 in the fluid (mol m^{-3}), and ΔHP is the hydrostatic pressure
103 gradient across the structure (kg m^{-1} sec^{-2}). Some examples in mammals illustrate how
104 morphology scales for structures relying on advection. In mammals, the radius of the aorta scales
105 with $mass^{0.375}$, and the length of the aorta scales with $mass^{0.25}$, suggesting that G_{adv} of the aorta
106 scales with $mass^{1.25}$ (4 * 0.375 – 0.25) (21). The tracheal-bronchial system is the advective
107 structure for air transport in vertebrates; radius scales with $mass^{0.39}$ while lengths scale with

108 mass$^{0.27}$, suggesting that G_{adv} for mammalian aorta and bronchial systems scale with mass$^{1.29}$
109 (22). G_{diff} for these same structures, on the other hand, scale as mass$^{0.5}$. Thus, the morphological
110 structures of mammalian respiratory systems seem to scale such that advective capacities
111 increase more than metabolic rates in larger species, while diffusive capacities decline. Of
112 course, mammalian oxygen transport through the bronchial tree and circulatory system is thought
113 to rely on advection regardless of size.

114 The design of the insect tracheal system is fundamentally different from either the
115 vertebrate respiratory system or that of skin-breathing aquatic invertebrates; and it remains
116 unclear how the components of the system scales. In insects, spiracles provide a (usually) gated
117 opening to an air-filled conduit system that branches through the insect, with oxygen transported
118 in the gas phase to the most distal surface of the tracheoles, with transport then occurring in the
119 liquid phase from tracheole to mitochondria (23). Since Krogh's demonstration that diffusion
120 should suffice for oxygen transport in a relatively large Lepidopteran larvae, diffusion has been
121 considered to be an important mechanism of gas exchange in insects (24, 25). However, many
122 insects, including small ones, supplement diffusion with advection, especially when active (23,
123 26, 27). The spiracles are potentially an important step in insect gas exchange, since they are
124 relatively small (difficult to see by eye in most insects) and yet must sustain all gas flux. It
125 appears that spiracle morphology just matches gas exchange needs at peak metabolic
126 performance with little additional capacity; for example, sealing of just one thoracic spiracle
127 reduces flight metabolic rate in *Drosophila* (28). At present it is not clear whether the size of
128 spiracles should best match G_{diff}, G_{adv} or some other physiological capacity. To shed light on this
129 question, we used micro-computed tomography (micro-CT) (29) to provide the first interspecific

examination of the scaling of spiracles, using ten species of scarab beetles spanning two orders of magnitude in mass, including some of the most massive extant species.

Methods

Acquisition of raw micro-CT images

Seventeen individuals of ten species (1-2 individuals per species) of scarab beetles (Fig. 1a) with a size range from 0.097 to 18 grams were obtained via breeders from online sources. We examined the following species: *Goliathus goliathus*, *Coelorrhina hornimani*, *Dicronorrhina derbyana*, *Mecynorrhina torquata*, *Eudicella euthalia*, *Protaetia orientalis*, *Popilia japonica*, *Trypoxylus dichotomus*, *Dynastes hercules*, and *Cyclocephalis borealis*. Most species had both male and females represented. Most specimens were scanned using a micro-CT scanner (Skyscan 1172, Bruker, Bilerica, MA, USA) equipped with a Hammamatsu 1.3 MP camera and Hammamatsu SkyScan Control software at Virginia Tech. To maintain tracheal structure in their natural configuration, we used a minimal preparation of fresh samples (30). All beetles were killed using ethyl acetate fumes, stored at 4 °C, and scanned within three days. They were warmed back to room temperature to avoid motion artifacts from fluid flow, placed in X-ray translucent polyimide tubing (Kapton, Dupont), and centered on a brass stage with putty. Power was set at 10 W, voltage was adjusted for optimum brightness and contrast (70-96 kV), with currents between 104-141 μA. Beetles were scanned with 0.4° rotation steps for 180° with frame averaging. A flat-field correction was applied to all scans to account for subtract aberrations. All raw projection images were collected a size of 1024 x 1280 pixels, yielding a scaling of 12-98 μm/pixel that was independent of beetle size. Average measured spiracle dimensions for width/height/depth for the smallest beetles were around 10 pixels and hence resolvable with minimally 10% resolution. Small beetles could be captured in a single scan, but larger beetles

were scanned sequentially in segments along their longitudinal axis by varying their position relative to the beam.

Dynastes hercules were too large to be scanned with the same instrument, so these beetles were imaged using an in-house-built bench-top micro-focus X-ray computed tomography (micro-CT) platform (see (31, 32) for details) at Virginia Tech. The X-ray tube (Oxford Instrument, Inc.) was operated at 70 kV and tube power was fixed at 20 W. Images were collected with an X-ray flat-panel detector (model C7921, Hamamatsu, Inc.) operated at 1x1 binning mode, with a detector element size of 50 x 50 µm. The axial scanning field-of-view (FOV) was 37.2 mm in diameter. In each scan, images were collected at 0.5° intervals as the beetle was rotated through 360°, resulting in a total of 720 X-ray projections per scan. Because the specimen was larger than the field of view, multiple scans were conducted sequentially along the animal's anterior-posterior axis to image the entire body. The axial slice images were reconstructed using the standard filtered back-projection (FBP) reconstruction algorithm, with an image matrix of 1008 x 1012 px and an isotropic pixel size of 36.8 x 36.8 µm.

Image Reconstruction and Measurements

Raw micro-CT images were imported into NRecon reconstruction software from SkyScan (Bruker, Bilerica, MA, USA). Ring artifact and beam hardening corrections were applied where necessary, and contrast was optimized using the software's interactive histogram feature. For large beetles that required multiple scans, reconstructions were set to align and fuse automatically. Slices generated in NRecon were imported into Avizo 9 software (ThermoFisher Scientific, Waltham, MA, USA) for 3D reconstructions.

Spiracles were identified by the characteristic slit-like shape of the opening, and the bellows-shaped air sac behind it (Figure 1b, 1c, 1d). Spiracle locations were confirmed by

dissection on representative specimens. Measurements were taken for one of the paired six abdominal and two thoracic spiracles for each beetle (Figure 1b,1c). A few scans had small aberrant regions (e.g., blurriness) due to challenges in scanning, so which spiracle was measured varied between the symmetric right and left side of an animal based on which region of the scan was best resolved. Diameters of the spiracular opening were measured at the widest point of opening to the outside air in the transverse and sagittal planes. Area of the opening was then calculated assuming an elliptical shape, with the lengths of the semi-major/minor axes being the diameters measured in the transverse and sagittal planes (Figure 1d). The depth of the spiracle was measured from the outer opening to the interior valve connecting the spiracle to the tracheal trunk (Figure 1d). The sex, mass and dimensions of all measured spiracles are provided in supplementary tables 1 and 2.

Calculations and Statistical Analyses

We measured the scaling relationships for each spiracle separately, using log-log plots. As dependent variables in these regressions, we tested $\log_{10}$ transformed spiracular depth, area, area/depth (as an index of the diffusive capacity of the spiracle, see Eq. 1), and area^2/depth (as an index of the resistance of the spiracle to advective flow, see Eq. 3).

We used two statistical approaches to assess the role of the phylogenetic relatedness of the animals in scaling patterns: a phylogenetic generalized linear model (pGLS) and a generative Bayesian model. We ran and plotted pGLS results in R (33-39). The goal of pGLS is to account for non-independence of data points due to phylogenetic relatedness in construction of the linear model, which requires a phylogeny of the study species (40). We spliced together such a phylogeny from multiple published scarab phylogenies. The branch positions for beetle subfamilies (Dynastinae, Rutelinae and Cetoniinae) were determined using Hunt et al. (41*)*. The

199 branches within Dynastinae were placed in the tree using work from Rowland and Miller (42),
200 and the branches of Cetoniinae determined with two trees, one from Mico et al. (43, 44) and the
201 other Holm (43, 44). Four of the genera in this study were present in the tree for Coleoptera
202 constructed by Bocak et al. (45), which indicated the same branch places as our spliced tree,
203 providing some positive confirmation for this tree structure. Branch lengths were set to a value of
204 one because actual branch lengths are not known. Similar to pGLS, we built a Bayesian model
205 assuming that the data were generated by a multivariate normal distribution with the covariance
206 matrix given by the amount of shared ancestry between species (amount of shared branch
207 length). See supplemental methods for the details of the model, selection of priors, and python
208 code. Detailed information on the analysis is available at the website for the paper here:
209 https://julianmwagner.github.io/spiracle_scaling/ and at the corresponding repository
210 (https://github.com/julianmwagner/spiracle_scaling). Analyses indicated that the parameter
211 characterizing the degree of phylogenetic signal in our data (λ) was non-identifiable
212 (supplemental figures 1,2); this result means that our data does not inform this parameter and it
213 could take on any value from zero (no phylogenetic signal) to one (strong phylogenetic signal)
214 with similar probability. Hence, we opted to omit the use of phylogenetic covariance from our
215 models since 1) the total non-identifiability made selecting a single λ via maximum likelihood
216 for the frequentist pGLS dubious, and 2) including it added no explanatory value to our Bayesian
217 regression (parameter samples for λ were essentially straight from the prior). We instead used
218 nonparametric bootstrapping (10,000 bootstrap replicates with ordinary least squares regression
219 slopes/intercepts/residual standard deviation as the summary statistics) to obtain confidence
220 intervals for our slope and intercept values. Additionally, we performed a Bayesian linear
221 regression. Our model was a normal likelihood with mean given by a line with slope and

intercept parameters. To obtain parameter estimates, we sampled using the Stan implementation of Hamiltonian Monte Carlo (cmdstanpy) in Python. See supplemental methods for the details of the model, selection of priors, and Python code and at the paper website/repository listed above. No data were excluded.

We defined isometric scaling as scaling as follows:

$mass^{0.67}$ for areas

$mass^{0.33}$ for area/depth

$mass^{1}$ for $area^{2}$/depth,

according to basic principles of geometric similarity (assuming mass is proportional to volume). We observed whether the 95% confidence interval given by bootstrapping/parameter samples for the slope of our measures of spiracle morphology overlapped with the isometric prediction. To produce any *p* values, we calculated the number of bootstrap replicates with test statistic at least as extreme as a particular value of interest, e.g. slope compared to isometry.

The diffusive capacity of a spiracle (G_{diff}, nmol sec^{-1} kPa^{-1}) at 25°C was calculated using equation 1, with K calculated as D * β, with D (the diffusivity constant for O_2 in air) = 0.178 cm^2 sec^{-1} (46) and β (the capacitance coefficient for oxygen in air) = 404 nmol cm^{-3} kPa^{-1} (47). The ΔPO_2 across the spiracles if gas exchange occurs completely by diffusion was calculated for various oxygen consumption rates using equation 2. Advective capacity was calculated using equation 3, assuming a dynamic viscosity of air of 1.86 x 10^{-8} kPa sec (46). To calculate total diffusive or advective capacity per beetle, the diffusive/advective capacity for all eight spiracles was summed and doubled (to obtain the total for both sides of the animal).

To calculate the ΔPO_2 across the spiracles needed to supply the beetle's total resting metabolic demand by diffusion, the metabolic rate for a quiescent beetle at a body temperature of

25 °C of a given mass was estimated from (48) with the following equation: $\log_{10}$(metabolic rate (μW)) = 3.2 + 0.75•$\log_{10}$(mass (g)). This metabolic rate was converted to an oxygen consumption rate assuming an RQ of 0.85 (20.7 μj nL^{-1}).

Estimating the scaling of gas exchange during flight of flying beetles has uncertainties. Niven and Scharlemann calculated a scaling coefficient for insect flight of 1.07 (49). Duell and Harrison recently re-assessed the scaling of flight metabolism in insects, and found that the scaling coefficients for flight metabolic rates depended on insect size, with a scaling coefficient of 1.19 for insects weighing less than 58 mg and of 0.67 for insects weighing more than 58 mg (50). As all of the beetles used in this study were larger than 58 mg, it seems likely that their flight metabolic rates scale hypometrically, with a slope less than 1. Scaling patterns can vary across clades (51, 52), so ideally, we would employ measures of the flight metabolic rates of the scarab beetles in this study. Unfortunately, most beetles cannot sustain flight in the small containers required for respirometry. Flight metabolic rates have as yet only been reported for four species (50), and the slope of the scaling relationship for these four species has great uncertainty. Thus, based on the current literature, the scaling exponent flight metabolic rates in insect likely ranges between 0.67 and 1.19, depending on size.

For calculations of the partial pressure gradient across the spiracles during flight, a critical factor is the magnitude of the aerobic scope. Three studies to date measured resting and flight metabolic rates for beetles ranging in body mass from 0.3 to 1.3 g; two used tethered flight and one free flight (53-55). Because it is challenging to induce maximal flight performance and measure aerobic metabolic rate, and we are interested in what the oxygen partial pressure gradient might be across the spiracles during maximal flight performance, we used the highest aerobic scopes reported for individual beetles in these studies, which were 80, 90 and 110x

higher than resting metabolic rates. We used the median of these values (90x) to estimate maximal aerobic metabolic rate during flight relative to quiescent 1 gram beetles. Because there is uncertainty in the scaling of metabolic rates during flight, the required PO_2 gradient across the spiracles to support gas exchange by diffusion at rest and during flight was calculated by rearranging equation 2 and performing unit conversions as follows:

$$(5)\ \Delta PO_2\ (\text{kPa}) = \left(\frac{\left(10^{\log_{10}(AS) + 3.20 + EXP * \log_{10}(\text{mass (g)})}\ \mu\text{W}\right)\left(\frac{1\ \frac{\mu\text{J}}{\text{s}}}{1\ \mu\text{W}}\right)\left(\frac{\text{nL}}{20.7\ \mu\text{J}}\right)\left(\frac{1\ \text{nmol}}{24.5\ \text{nL}}\right)}{\left(\frac{\text{area}}{\text{depth}}\ (\text{cm})\right)\left(0.178\ \frac{\text{cm}^2}{\text{sec}}\right)\left(404\ \frac{\text{nmol}}{\text{cm}^3\text{kPa}}\right)} \right).$$

where conversion factors of 20.7 kJ/L and 24.5 mol/L were assumed for O_2 at 25 °C, AS is the aerobic scope (1 for resting [$\log_{10}(1)=0$ in the equation] and 90 for a flying 1 g insect [$\log_{10}(90)=1.954$ in the equation]), and EXP is the scaling exponent for metabolic rate.

Results

All spiracles scaled with geometric isometry for area, depth, area/depth (which corresponds to diffusive capacity), and area^2/depth (which corresponds to advective capacity) (figure 2, supplemental figures 3-7, supplementary tables 3 and 4). Some example regressions with confidence intervals for the slopes are shown in figure 2, illustrating scaling isometry, the larger size of the mesothoracic spiracle, and the tight size distribution of the more anterior spiracles as compared to the posterior; regressions and confidence intervals for each spiracle are in supplementary table 4. The mesothoracic spiracle was much larger than any of the other spiracles, consistent with the general trend of increasing spiracular area closer to the anterior of the animal (supplemental figure 3, supplementary table 3). The area of the mesothoracic spiracles was approximately four times larger than both the metathoracic spiracles, and abdominal spiracles 1-3, and abdominal spiracles 4-6 were approximately half the size of the

more anterior abdominal spiracles (supplemental figure 3). Not only were anterior spiracles larger than posterior, but they also had much lower variability around the trend line within the species assayed in this study (figure 2a,b,c). In comparison, the depth of the spiracles showed much less variability in tightness of the distribution around the scaling trend lines (figure 2d,e,f).

As with individual spiracles, the combined diffusing capacity of all the spiracles scaled isometrically, with a slope not significantly different from 0.33 (Fig. 3a, Supplementary table 5). The upper 95% confidence limit for this slope was 0.505, well less than any reported interspecific scaling exponent for metabolic rate. For resting metabolic rate, (slope of 0.75, shown as the repeated light grey background lines), the required pO_2 gradient across spiracles necessary to supply oxygen by diffusion was small but increased by an order of magnitude, from about 0.05 kPa in the smallest beetles to nearly 0.5 kPa in the largest scarabs (Fig. 3b). For flight, we present the scaling of the required pO_2 gradient across spiracles necessary to sustain maximal aerobic flight metabolic rate by diffusion for two situations, if flight metabolic scales with an exponent of 0.67 or 1.19. For small beetles, the estimated pO_2 gradient across spiracles during flight was 2 - 5 kPa. Thus, plausibly, beetles in the smallest size range may be able to deliver sufficient oxygen to the tissues by diffusion, though further studies of conductance of the tracheal system between the spiracles and flight muscles will be required to answer this question. For the largest beetles, the required pO_2 gradient across spiracles during flight substantially exceeded 21 kPa, indicating that during maximal aerobic flight performance, diffusion cannot supply oxygen across the spiracles, and certainly not to the flight muscles (Fig. 3b, Supplementary table 5). Regardless of whether flight metabolic rate scales with an exponent of 0.67 or 1.19, because metabolic rates increase more with size than spiracular diffusing capacity,

the required pO_2 gradient across spiracles increases with body size for diffusive gas exchange (Fig. 3b).

In contrast, the advective capacity increased with an estimated slope of 1.1, that was greater (95% confidence limits 0.84 – 1.34) than the minimum scaling exponent for flight metabolic rate (0.67), also greater than the estimated slope of metabolic rate for resting insects (slope of 0.75, light grey lines), but included maximum scaling exponent reported for flight metabolic rates in insects (1.19, Fig. 3c).

Discussion

Spiracles scaled with geometric isometry. Isometric scaling of diffusive capacities means that diffusion becomes increasingly less able to meet oxygen demands in larger beetles, with the required gradient for oxygen transport by diffusion through the spiracles increasing by an order of magnitude over two orders of magnitude in body mass. Conversely, our data demonstrate that the advective capacities of the spiracles scale more positively than resting metabolic rates. For flight metabolic rates, uncertainties in the scaling exponent for flight metabolic rates of beetles means that we can only conclude that the scaling exponents for advective capacities of the spiracles may match or possibly exceed those of metabolic rates. These results demonstrate that large insects must rely on advection through the spiracles in order to achieve their maximal aerobic flight metabolic rates. Our results also imply that there is no physical constraint associated with spiracular gas exchange that limits insect size and metabolic rates.

It is important to note that our analysis only assessed required pO_2 gradient across spiracles, not within the entire tracheal system. Within the body of insects, gases must be transported through the large tracheal trunks, and then down the branching smaller tracheae and tracheoles in the gas phase, and then finally through liquid phases in the ends of the tracheoles

and from the tracheoles to the mitochondria. As yet, we have little information on the relative resistances of these various steps. Based on the P_{CO2} gradient between the spiracles and tracheal trunks, and between the tracheal trunks and the hemolymph (perhaps similar to cellular P_{CO2}), the resistance of the internal tracheal system to CO_2 transport to active muscles likely substantially exceeds that of the spiracles in active, locomoting animals, whereas spiracular and tracheal resistances may be similar in resting animals (56). This raises the interesting question of whether large insects can supply their resting metabolic rate by diffusion alone. The fact that the calculated required P_{O2} gradient across the spiracles required to sustain resting metabolic rate for the largest beetles in this study is only 0.5 kPa would suggest that the answer is yes. This conclusion is supported by our experience (unpublished observations) that even very large larval and adult scarab beetles (> 30 g) can recover from anoxia, which strongly suggests that diffusion can sustain at least the minimal aerobic metabolic rate necessary to restart ventilation.

While the spiracles scale isometrically in beetles, this pattern does not occur universally for tracheal structures, or consistently across clades. Comparing tenebrionid beetles inter-specifically, the leg tracheae scale hypermetrically, but the head tracheae scale isometrically (6). Within a bumblebee species, one spiracle scales isometrically (16). In the leg of growing locust (*Schistocerca americana*), the diffusing capacity of the large longitudinal tracheae of the leg scales hypometrically (17), whereas in a growing caterpillar (*Manduca sexta*), diameters of most tracheae scale isometrically (57). Why different scaling patterns are observed in these different cases is unclear; more in-depth analysis of the required gas transport and the mechanism of transport are needed to evaluate the scaling of individual tracheal system structures. Plausibly the various steps in gas exchange scale similarly (a hypothesis of symmorphosis) as has been

356 suggested for mammalian respiratory systems (58), but resolution of this question in insects will
357 require further study.

358 Diffusive capacities of the spiracles scaled with mass$^{0.39}$, well below the scaling slope for
359 resting oxygen consumption rate (approximately 0.75); thus, diffusion across the spiracles
360 becomes more challenging for larger insects. The required O_2 gradient across the spiracles to
361 supply the metabolic demand by diffusion increases by approximately an order of magnitude
362 from our smallest to largest beetles, but the size effect on the required PO_2 gradient is less
363 important than the effect of activity. For quiescent beetles, the PO_2 gradients across the spiracles
364 necessary for diffusion are low (0.05-0.5 kPa depending on size). However, during endothermic
365 flight, the required PO_2 gradient across the spiracles increases from 5 to 35 kPa for a scaling
366 exponent of 0.67 or from 2 to 174 kPa for a scaling exponent of 1.19, which is impossible to
367 achieve because the maximum partial pressure of oxygen in air is only 21 kPa. With metabolic
368 rates scaling with mass$^{0.75}$ and spiracular depth with mass$^{0.33}$, spiracular area would need to scale
369 with mass$^{1.08}$ (0.75 + 0.33) to conserve the required PO_2 gradient to support diffusion across all
370 insect sizes.

371 By contrast, advective capacity scales with mass$^{1.1}$, exceeding or matching the scaling of
372 flight metabolic rate, depending on insect size (50). Interpretation of these results is challenging
373 as we do not know how ventilatory flow varies with size in insects. Ventilatory airflow is
374 difficult to measure in insects, because there are so many spiracles, because these spiracles can
375 be variably gated, and because flow can be tidal or unidirectional. If insects can match
376 ventilation to flight metabolic rate across body size, then no changes in oxygen extraction
377 efficiency will be necessary. If ventilatory airflow is matched to flight metabolic rate, then the
378 scaling of advective capacities of the spiracles with an exponent of 1.1 implies that the pressures

379 required to drive convection either remain the same with size (if flight metabolic rate scales with
380 an exponent near 1.1) or falls with size (if flight metabolic rate scales with an exponent of 0.67
381 or 0.75, for example. Any conclusions on this topic must be very cautious because in the beetles
382 that have been best-studied, ventilation during flight includes both tidal flow through some of the
383 thoracic spiracles and unidirectional flow out the abdominal spiracles (59). The much larger size
384 of the thoracic than abdominal spiracles suggests that ventilation of the flight muscles may be
385 primarily tidal through the thoracic spiracles, with unidirectional flow out the abdominal
386 spiracles supplying other parts of the body.

387 We also observe much tighter distributions in the scaling pattern for the area of the large
388 anterior spiracles as compared to the smaller posterior ones. This result may suggest that the
389 large anterior spiracles are more constrained in their morphology, since they presumably provide
390 the gas exchange needed for metabolically demanding tissues like the flight muscle.

391 There are some important caveats when interpreting our data. Insect spiracles are
392 morphologically complex structures. We made 3D measurements using tomographic imaging,
393 but analyzed air transport capacities by modeling the spiracle as a cylinder, which could over or
394 underestimate capacity depending on factors like valve position and the complex shape of the
395 spiracular atrium. Furthermore, our CT scans were conducted on sacrificed specimens; the
396 assessment of spiracles of living insects could offer insights not possible with static morphology.
397 For example, living insects might control the shape of the bellows-like atrium and valves in a
398 concerted way to promote air flow. As yet, we know little about how the tracheal system
399 structure and function might scale differently in different species. As an example of a fairly
400 dramatic difference in tracheal system function across beetle clades, some Cerambycid beetles
401 use draft inward ventilation through the mesothoracic spiracle during flight, whereas most scarab

beetles autoventilate the thorax using wing movements (59, 60). Dung beetle species vary between exhaling nearly all to none of their air out the mesothoracic spiracles, with species from more arid environments exhibiting more expiration via the mesothoracic spiracle (61). Multiple beetle species collapse parts of their tracheal system to produce advective airflow, both in adults and as pupae (62-64). Though it is unclear how respiration via tracheal collapse differs with size and in different species, the prevalence of active breathing further highlights the need for advective airflow for insect function. The phylogenetic, life history, and environmental influences on tracheal system structure, function, and scaling seem likely to be a ripe area for future research.

Our finding of isometric scaling of insect spiracles would appear to differ from reports for tracheae of mammals, in which radius scales with mass$^{0.39}$ and lengths with mass$^{0.27}$ (65). However, confidence limits from our study included these scaling slopes, suggesting that respiratory scaling of tracheal morphology may be congruent across these disparate groups. Tenney and Bartlett's study (65) had greater power, as it examined 43 species ranging over 5 orders of magnitude in body mass. However, it worth noting that they did not consider error in their slope estimates, test for statistical differences in slopes between the radii and lengths, or consider phylogeny, so the conclusion that mammalian tracheae scale non-isometrically (and differently from insect spiracles) could benefit from rigorous comparative analysis.

Conclusions: Insect spiracles scale with geometric isometry in beetles, which means that diffusive capacities increase much less than metabolic rates as body size increases, while advective capacities increase similarly or more rapidly than do metabolic rates. These are general principles of gas exchange that should apply to respiratory structures of any animal clade exhibiting isometric scaling. For resting insects, the required P_{O2} gradient across the spiracles

425 necessary to supply resting oxygen consumption increases strongly with size, but remains small
426 in even the largest insects, suggesting that resting gas exchange can be accomplished by
427 diffusion even in very large insects. In contrast, our data clearly demonstrate that maximal
428 aerobic flight cannot be accomplished by diffusion in large beetles.

429 **Authors' contributions**

430 JW helped with study design, collected spiracle measurements from the micro-CT data,
431 carried out statistical analyses, and drafted the manuscript and figures. JFH helped with study
432 design, coordinated the study, and drafting the manuscript. CJK and JJS collected the micro-CT
433 data; additionally, *Dynastes* data were collected in collaboration with HG and GC. MED helped
434 develop methods for analysis of micro-CT data, and helped with phylogenetic correction
435 analysis. JJS also helped draft the manuscript. All authors gave approval for publication.

436 **Funding**

437 This research was supported in part by funds from the School of Life Sciences
438 Undergraduate Research (SOLUR) Program through the School of Life Sciences at Arizona
439 State University, Tempe Campus, and by NSF IOS 1122157 and 1558052.

References

1. Bonner JT. Why size matters: from bacteria to blue whales. Princeton, N.J.: Princeton University Press; 2006.
2. West GB. Scale: The Universal Laws of Growth, Innovation, Sustainability, and the Pace of Life in Organisms, Cities, Economics, and Companies. New York: Penguin Press; 2017.
3. Sibly RM, Brown JH, Kodric-Brown A. Metabolic Ecology: A Scaling Approach: Wiley-Blackwell; 2012.
4. West GB, Brown JH, Enquist BJ. A general model for the origin of allometric scaling laws in biology. Science. 1997;274:122-6.
5. Gillooly JF, Gomez JP, Mavrodiev EV, Rong Y, McLamore ES. Body mass scaling of passive oxygen diffusion in endotherms and ectotherms. Proceedings of the National Academy of Sciences. 2016;113(19):5340-5.
6. Kaiser A, Klok CJ, Socha JJ, Lee W-K, Quinlan MC, Harrison JF. Increase in tracheal investment with beetle size supports hypothesis of oxygen limitation on insect gigantism. Proceedings of the National Academy of Sciences. 2007;104(32):13198-203.
7. Lane SJ, Shishido CM, Moran AL, Tobalske BW, Arango CP, Woods HA. Upper limits to body size imposed by respiratory–structural trade-offs in Antarctic pycnogonids. Proceedings of the Royal Society B: Biological Sciences. 2017;284(1865).
8. Perry SF, Lambertz M, Schmitz A. Respiratory Biology of Animals. Evolutionary and Functional Morphology. Oxford, U.K.: Oxford Press; 2019.
9. Banavar JR, Moses ME, Brown JH, Damuth J, Rinaldo A, Sibly RM, et al. A general basis for quarter-power scaling in animals. Proceedings of the National Academy of Sciences. 2010;107(36):15816-20.
10. Glazier DS. Metabolic scaling in complex living systems. Systems. 2014;2(4):451-540.
11. Harrison JF. Do performance-safety trade-offs cause hypometric metabolic scaling in animals? Trends Ecol Evol. 2017;32(9):653-64.
12. Harrison JF. Approaches for testing hypotheses for the hypometric scaling of aerobic metabolic rate in animals. American Journal of Physiology-Regulatory, Integrative and Comparative Physiology. 2018;315(5):R879-R94.
13. White CR, Kearney MR. Metabolic scaling in animals: methods, empirical results, and theoretical explanations. Comprehensive Physiology. 2014;4:231-56.
14. Peters RH. The Ecological Implications of Body Size. Cambridge: Cambridge University Press; 1983.
15. Harrison JF, Kaiser A, VandenBrooks JM. Atmospheric oxygen level and the evolution of insect body size. Proceedings of the Royal Society B-Biological Sciences. 2010;277(1690):1937-46.
16. Vogt JF, Dillon ME. Allometric scaling of tracheal morphology among bumblebee sisters (Apidae: *Bombus*): compensation for oxygen limitation at large body sizes? Physiol Biochem Zool. 2013;86.
17. Harrison JF, Lafreniere JJ, Greenlee KJ. Ontogeny of tracheal dimensions and gas exchange capacities in the grasshopper, Schistocerca americana. Comparative Biochemistry and Physiology a-Molecular & Integrative Physiology. 2005;141(4):372-80.
18. Greenlee KJ, Henry JR, Kirkton SD, Westneat MW, Fezzaa K, Lee WK, et al. Synchrotron imaging of the grasshopper tracheal system: morphological components of tracheal hypermetry and the effect of age and stage on abdominal air sac volumes and convection. American Journal of Physiology: Comparative, Regulatory and Integrative Physiology. 2009;297:1343-50.
19. Ar A, Rahn H. **Pores in avian eggshells: gas conductance, gas exchange and embryonic growth rate**. Respir Physiol. 1985;61(1):1-20.

20. Toien O, Paganelli CV, Rahn H, Johnson RR. Diffusive resistance of avian eggshell pores. Respir Physiol. 1988;74:345-54.
21. Holt JP, Rhode EA, Holt WW, Kines H. Geometric similarity of aorta, venae cavae, and certain of their branches in mammals. Am J Physiol. 1981;241:100-4.
22. Stahl WR. Scaling of respiratory variables in mammals. J Appl Physiol. 1967;22(3):453-60.
23. Harrison JF, Wasserthal LT, Chapman RF. Gaseous exchange. In: Simpson SJ, Douglas AE, editors. The Insects: Structure and Function. 5th ed. New York: Cambridge University Press; 2013. p. 501-45.
24. Krogh A. Studien über Tracheenrespiration. II. über Gasdiffusion in den Tracheen. Pflügers Archiv. 1920;179:95-112.
25. Hetz SK, Bradley TJ. Insects breathe discontinuously to avoid oxygen toxicity. Nature. 2005;433(7025):516-9.
26. Socha JJ, Forster TD, Greenlee KJ. Issues of convection in insect respiration: Insights from synchotron X-ray imaging and beyond. Respir Physiol Neurobiol. 2010;173S:S65-S73.
27. Wasserthal LT, Cloetens P, Fink RH, Wasserthal LK. X-ray computed tomography study of the flight-adapted tracheal system in the blowfly *Calliphora vicina*, analysing the ventilation mechanism and flow-directing valves. J Exp Biol. 2018;221:1-12.
28. Heymann N, Lehmann F-O. The significance of spiracle conductance and spatial arrangement for flight muscle function and aerodynamic performance in flying *Drosophila*. J Exp Biol. 2006;209(9):1662-77.
29. Iwan D, Kamiński MJ, Raś M. The Last Breath: A µCT-based method for investigating the tracheal system in Hexapoda. Arthropod Struct Dev. 2015;44(3):218-27.
30. Socha JJ, DeCarlo F. Use of synchrotron tomography to image naturalistic anatomy in insects. SPIE 2008;2008(Developments in X-Ray Tomography VI: San Diego, CA, USA):70780A-7.
31. Sharma KS, Gong H, Ghasemalizadeh O, Yu H, Wang G, Cao G. Interior micro-CT with an offset detector. Medical Physics. 2014;41(6):061915.
32. Gong H LJ, Zhou O, & Cao G Medical Imaging 2015: Physics of Medical Imaging, (International Society for Optics and Photonics), p 94124N, editor Implementation of interior micro-CT on a carbon nanotube dynamic micro-CT scanner for lower radiation dose. SPIE Medical Imaging; 2015.
33. Garnier S. Paxkage 'viridis' 2016 [Available from: https://cran.microsoft.com/snapshot/2016-08-05/web/packages/viridis/viridis.pdf.
34. Orme D. The caper package: comparative analysis of phylogenetics and evolution in R 2018 [Available from: https://cran.r-project.org/web/packages/caper/vignettes/caper.pdf.
35. Pinheiro J, Bates D, DebRoy Sa, Sarkar D, Team RC. Linear and Nonlinear Mixed Effects Models 2021 [Available from: {https://CRAN.R-project.org/package=nlme}.
36. Harmon LJ, Weir JT, Brock CD, Glor RE, Challenger W. GEIGER: investigating evolutionary radiations. Bioinformatics. 2008;24.
37. Revell LJ. phytools: an R package for phylogenetic comparative biology (and other things). Methods Ecol Evol. 2012;3.
38. Paradis E, Claude J, Strimmer K. APE: Analyses of Phylogenetics and Evolution in R language. Bioinformatics. 2004;20(2):289-90.
39. R-Core-Team. R: A language and environment for statistical computing Vienna, Austria: R Foundation for Statistical Computing; 2016 [Available from: http://www.R-project.org/.
40. R. P. Freckleton, P. H. Harvey, M. Pagel. Phylogenetic Analysis and Comparative Data: A Test and Review of Evidence. The American Naturalist. 2002;160(6):712-26.
41. Hunt T, Bergsten J, Levkanicova Z, Papadopoulou A, John OS, Wild R, et al. A comprehensive phylogeny of beetles reveals the evolutionary origins of a superradiation. Science. 2007;318(5858):1913-6.

42. Rowland JM, Miller KB. Phylogeny and systematics of the giant rhinoceros beetles (Scarabaeidae: Dynastini). Insecta Mundi 2012;0258-0263:1-15.
43. Holm E. On the genera of African Cetoniinae: Anisorrhina Westwood 1842, Melinesthes Kraatz 1880 and Inhambane Péringuey 1907. Tropical Zoology. 1993;6(1):165-77.
44. Micó E, Morón MA, Šípek P, Galante E. Larval morphology enhances phylogenetic reconstruction in Cetoniidae (Coleoptera: Scarabaeoidea) and allows the interpretation of the evolution of larval feeding habits. Syst Entomol. 2008;33(1):128-44.
45. Bocak L, Barton C, Crampton-Platt A, Chesters D, Ahrens D, Vogler AP. Building the Coleoptera tree-of-life for >8000 species: composition of public DNA data and fit with Linnaean classification. Syst Entomol. 2014;39(1):97-110.
46. Lide DR, editor. CRC Handbook of Chemistry and Physics. 72 ed. Boca Raton: CRC Press; 1991.
47. Piiper J, Dejours P, Haab P, Rahn H. Concepts and basic quantities in gas exchange physiology. Respir Physiol. 1971;13:292-304.
48. Chown SL, Marais E, Terblanche JS, Klok CJ, Lighton JRB, Blackburn TM. Scaling of insect metabolic rate is inconsistent with the nutrient supply network model. Funct Ecol. 2007;21:282-90.
49. Niven JE, Scharlemann JPW. Do insect metabolic rates at rest and during flight scale with body mass? Biol Lett. 2005;1:346-9.
50. Duell ME, Klok CJ, Roubik DW, Harrison JF. Size-dependent scaling of insect flight metabolism reveals an energetic benefit to small body size. Integr Comp Biol. 2022;In Press.
51. Ehnes RB, Rall BC, Brose U. Phylogenetic grouping, curvature and metabolic scaling in terrestrial invertebrates. Ecol Lett. 2011;14(10):993-1000.
52. Capellini I, Venditti C, Barton RA. Phylogeny and metabolic scaling in mammals. Ecology. 2010;91(9):2783-93.
53. Chappell MA. Thermoregulation and energetics of the green fig beetle (*Cotinus texana*) during flight and foraging behavior. Physiol Zool. 1984;57(6):581-9.
54. Rogowitz GL, Chappell MA. Energy metabolism of eucalyptus-boring beetles at rest and during locomotion: gender makes a difference. J Exp Biol. 2000;203:1131-9.
55. Auerswald L, Schneider P, Gäde G. Proline powers pre-flight warm-up in the African fruit beetle Pachnoda sinuata (Cetoniinae). J Exp Biol. 1998;201(10):1651-7.
56. Harrison JF. Ventilatory mechanism and control in grasshoppers. Am Zool. 1997;37:73-81.
57. Lundquist TA, Kittilson JD, Ahsan R, Greenlee KJ. The effect of within-instar development on tracheal diameter and hypoxia-inducible factors α and β in the tobacco hornworm, Manduca sexta. J Insect Physiol. 2018;106:199-208.
58. Weibel ER, Taylor CR, Hoppeler H. The concept of symmorphosis: a testable hypothesis of structure-function relationship. Proceedings of the National Academy of Science, USA. 1991;88:10357-61.
59. Miller PL. The supply of oxygen to the active flight muscles of some large beetles. J Exp Biol. 1966;45:285-304.
60. Amos WB, Miller PL. The supply of oxygen to the active flight muscles of Petrognathus gigas (F.) (Cerambycidae). Entomologist. 1965;98:88-94.
61. Duncan FD, Byrne MJ. The role of the mesothoracic spiracles in respiration in flighted and flightless dung beetles. J Exp Biol. 2005;208(5):907-14.
62. Pendar H, Kenny MC, Socha JJ. Tracheal compression in pupae of the beetle Zophobas morio. Biol Lett. 2015;11(6):20150259-.
63. Socha JJ, Lee W-K, Harrison JF, Waters JS, Fezzaa K, Westneat MW. Correlated patterns of tracheal compression and convective gas exchange in a carabid beetle. J Exp Biol. 2008;211(21):3409-20.

579 64. Waters JS, Lee WK, Westneat MW, Socha JJ. Dynamics of tracheal compression in the horned
580 passalus beetle. American Journal of Physiology: Regulatory, Integrative and Comparative Physiology.
581 2013;304:R621-R7.
582 65. Tenney SM, Bartlett D. Comparative quantitative morphology of the mammalian lung: Trachea.
583 Respir Physiol. 1967;3(2):130-5.

584

Figure Legends

Figure 1. Scarab beetles include large bodied individuals and have eight spiracles. (a) Phylogenetic tree for the scarab beetles used in this study showing size distribution among clades (branch lengths are meaningless). (b) Location of the eight spiracles in the scarab body. (c) 3D reconstruction of the tracheal trunks in the thorax, legs and abdomen of *Dicronorrhina derbyana*; spiracles are shown in white. The larger images of spiracles show the size of the opening (dark in color) compared to the mushroom-shaped (white) atrium behind and the differences in spiracle shape. (d) Transverse x-ray slice through the third abdominal spiracle with diameter, α, and depth, β, measures illustrated.

Figure 2. Isometric scaling of scarab beetle spiracles. Spiracle area scales with geometric isometry (A, B), with much tighter distribution about the isometric model for the large anterior spiracles compared to the smaller posterior spiracles. In A, B, D and E, the light grey lines show isometric scaling (slopes of 0.67 for area and 0.33 for depth). C shows estimates for the variability for regression models for the various spiracles (S mesothoracic, T metathoracic, 1-6 abdominal), calculated as the standard deviation divided by $10^{\text{regression intercept}}$, which represents the spiracle area for a 1g beetle. Black diamond and line show the median and 2.5^{th}-97^{th} residual standard deviation divided by $10^{\text{regression intercept}}$ calculated on non-parametric bootstrap samples. The white diamond and grey interval represent the median and 3^{rd}-97^{th} highest posterior density interval for the standard deviation divided by $10^{\text{regression intercept}}$ calculated from parameter samples from the Bayesian regression. We see a trend towards much higher variability in posterior spiracle area as compared to anterior. In contrast to spiracle area, spiracle depth shows similar variability in all spiracles (D-F) regardless of position.

Figure 3. Scaling of the spiracles is insufficient for diffusive capacities across the spiracles to match expected increases in metabolic rate, so for pure diffusive gas exchange, the required partial pressure for oxygen must increase with size. In contrast, advective capacities through the spiracles likely match or exceed the scaling of flight metabolic rate. (a) The $\log_{10}$ of total spiracular diffusive capacity per beetle (nmol s^{-1} kPa^{-1}) increases with beetle size, with a slope estimated as 0.39. This slope was not significantly different from the 0.33 predicted from isometric scaling. The upper 95% confidence limit for the slope was 0.505, lower than any reported metabolic scaling slopes for insects. A metabolic rate slope of 0.75, commonly found for resting insects and animals more generally, is shown in light grey. (b) The $\log_{10}$ PO_2 gradient (kPa) across the spiracles required to diffusively supply the oxygen demand of beetles increases with beetle size. The lower, purple line shows the estimated PO_2 gradient across the spiracles to support diffusive gas exchange at rest; this increases from approximately 0.05 to 0.49 kPa as beetles increase in body size across this range. The less steeply upward sloping greenish and steeper yellow lines shows the estimated PO_2 gradient across the spiracles during flight, assuming a 90x aerobic scope if flight metabolic rates scale with an exponent of 0.67 or 1.19, as found for large insects and small insects respectively (50). The upper grey band indicates where the partial pressure of oxygen needed for calculated beetle metabolic demand exceeds the 21 kPa atmospheric oxygen level (c) Hypermetric scaling of $\log_{10}$ summed advective capacity (m^3 s^{-1}•kPa^{-1}) versus $\log_{10}$(body mass). There are uncertainties in the scaling of metabolic rate in flying insects: depending on size and study, slopes have ranged from 0.67 to 1.19. Confidence limits for advecting capacity include 1.19 but not 0.67. Equations of regression lines and confidence intervals for the slopes are shown for each plot.

Supplemental Materials

Supplemental figure 1. Non-identifiability of phylogenetic signal parameter in pGLS regression model. Left-hand column shows both OLS regression and pGLS regression models plotted for a given spiracle morphology (log of area, depth, area/depth, or area^2/depth) vs log of mass. The Right-hand column shows the log likelihood space for the parameter λ, which scales the off-diagonal covariance terms of the regression model thereby providing an indication of how strongly phylogeny influences the pattern of data distribution. A λ of one indicates strong phylogenetic signal whereas a value of zero indicates no sign of covariance in the data due to phylogeny. The solid red line indicates the maximum likelihood for the parameter used in the model on the left, the dashed red line indicates confidence interval estimates for the parameter value. Note that the log likelihood for the parameter is fairly flat across large section of the possible parameter space, and all confidence intervals on the parameter include zero (no phylogenetic signal). Together, these indicate that many values for λ are similarly likely, and that the strength of the phylogenetic signal is hence non-identifiable (our data does not strongly inform the parameter). Given the weakly-to-non-peaked likelihood distributions, selecting a particular value for λ to use in the model is a largely arbitrary choice, poorly supported by the data.

Supplementary figure 2. Non-identifiability of the phylogenetic signal parameter as indicated by Bayesian modeling. We constructed a generative model for our data (a multivariate normal distribution with covariance matrix given by the phylogenetic signal) which is analogous to the model assumed in pGLS regression. We included a parameter for λ that scaled the off-diagonal terms of the covariance matrix, analogous to pGLS, and sampled from our model for the various

652 regressions of log spiracle morphology versus log mass. We then plotted the prior for the λ
653 parameter (a beta distribution with shape parameters 1.4 and 1.4) against the samples from HMC
654 sampling. This indicated that the samples for this parameter had no shrinkage: the posterior
655 samples for the parameter matched the prior. This indicates that the data does not inform this
656 parameter, a clear indication that the parameter is entirely non-identifiable given our data.
657 Together, with supplemental figure 1, this indicates that the phylogenetic signal is not
658 informative for our models and does not provide useful information or insight to our analysis.
659
660 Supplementary figure 3. Slopes, intercepts, standard deviations, and quasi-coefficient of
661 variation with confidence intervals generated via non-parametric bootstrapping or Bayesian
662 regression for all spiracles and area, depth, area/depth, or area^2/depth vs mass. All spiracles
663 scaled isometrically. The anterior spiracles are much larger than the posterior ones and hence
664 provide much of the gas exchange capacity for the animal. They also exhibit a much tighter
665 distribution for their area and gas exchange capacity than the posterior ones. The spiracle depth,
666 however, did not show the same level of variation in dimension; all spiracular depths had similar
667 degree of variation. This suggests there may be tighter selective regulation on the morphology of
668 the large spiracles that likely supply the airflow needed for highly metabolically demanding
669 tissue like the flight muscle, legs, and brain.
670
671 Supplementary figure 4. Regression plots for both Bayesian and non-parametric bootstrap
672 analyses. The top set of panels provide results for Bayesian linear regression; the light grey
673 bands provide the 80th and 95th percentile for the posterior predictive distribution for the
674 regression model, the dark grey interval shows the 95th percentile for regression line ranges given

675 by the slope and intercept samples, the black line the 10^{th} percentile for these regression lines.
676 The bottom panels show regression results from non-parametric bootstrap replicates drawn from
677 the data, with ordinary least squares regression as the summary statistic applied to the
678 subsamples. The grey interval shows the 95^{th} percentile for the regression lines generated by the
679 bootstrap sampling. The repeated light grey lines in both sets of figures indicate the theoretical
680 isometric slope value for the regression of a given morphological trait.
681
682 Supplementary table 1. The measurements made on each spiracle for each beetle.
683 Supplementary table 2. Area and depth measurements for each spiracle for each beetle.
684 Supplementary table 3. Conductances for diffusion and advection for each spiracle for each
685 beetle.
686 Supplementary table 4. Intercepts and slopes for scaling relationships (log-log plots) for
687 morphologies (spiracular areas and depths), conductances, and P_{O2} gradients across the spiracles,
688 including confidence limits, for each spiracle and for all spiracles combined.
689 Supplementary table 5. Summed spiracular areas and average spiracular depths, summed
690 conductances, and estimated average P_{O2} gradients across all the spiracles, for each beetle
691 species, estimated at rest and during flight if flight metabolic rate scale with $mass^{0.67}$ or $mass^{1.19}$.
692
693 Supplementary video: Reconstruction of the spiracles and connecting tracheal trunks on one side
694 of the scarab beetle *Dicronorhina derbyana*.
695

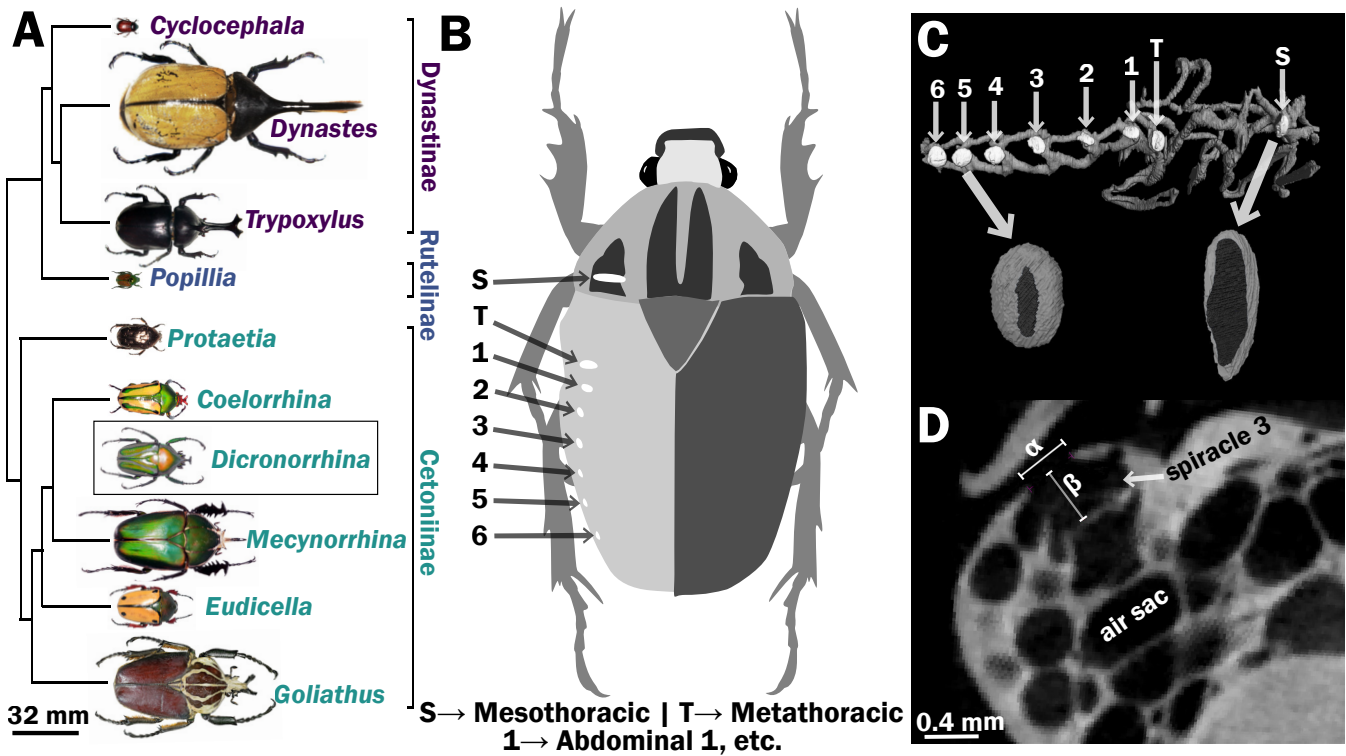
A
Cyclocephala
Dynastes
Trypoxylus
Popillia
Protaetia
Coelorrhina
Dicronorrhina
Mecynorrhina
Eudicella
Goliathus
Dynastinae
Rutelinae
Cetonilinae
32 mm
B
S
T
1
2
3
4
5
6
S→ Mesothoracic | T→ Metathoracic
1→ Abdominal 1, etc.
C
6
5
4
3
2
1
T
S
D
α
β
spiracle 3
air sac
0.4 mm